Measuring the aspect ratio renormalization of anisotropic-lattice gluons

M. Alford
Center for Theoretical Physics, Massachusetts Institute of Technology, Cambridge, Massachusetts 02139

I. T. Drummond, R. R. Horgan, and H. Shanahan
D.A.M.T.P., CMS, Wilberforce Road, Cambridge, England CB3 0WA

M. Peardon*
John von Neumann Institute for Computing and DESY, Forschungszentrum Jülich, D-52425 Jülich, Germany
(Received 27 March 2000; published 22 February 2001)

Using tadpole-improved actions we investigate the consistency between different methods of measuring the aspect ratio renormalization of anisotropic-lattice gluons for bare aspect ratios $\chi_0=4,6,10$ and inverse lattice spacing in the range $a_s^{-1}=660$–840 MeV. The tadpole corrections to the action, which are established self-consistently, are defined for two cases, mean link tadpoles in the Landau gauge and gauge invariant mean plaquette tadpoles. Parameters in the latter case exhibited no dependence on the spatial lattice size L, while in the former, parameters showed only a weak dependence on L easily extrapolated to $L=\infty$. The renormalized anisotropy χ_R was measured using both the torelon dispersion relation and the sideways potential method. There is general agreement between these approaches, but there are discrepancies which are evidence for the presence of lattice artifact contributions. For the torelon these are estimated to be $O(\alpha_S a_s^2/R^2)$, where R is the flux-tube radius. We also present some new data that suggest that rotational invariance is established more accurately for the mean-link action than the plaquette action.

DOI: 10.1103/PhysRevD.63.074501 PACS number(s): 11.15.Ha, 12.38.Gc, 12.39.Jh, 12.39.Mk

I. INTRODUCTION

In principle, an improved action makes it possible to achieve lattice volumes large enough to overcome finite-size effects at a computational effort low enough to obtain measurements with good statistical errors. However, typical masses for heavy states may be similar to or larger than the inverse lattice spacing on the associated coarse lattice. Propagators for such states then decay too fast in lattice units for accurate measurement.

The problem can be overcome by tuning couplings associated with the ''time'' direction so that the temporal lattice spacing a_t is much smaller than the spatial lattice spacing a_s. Refined measurements are then possible while retaining the computational advantages of the improved action and coarse spatial lattice. Such anisotropic actions have already been successfully applied to the glueball spectrum [1,2], the spectrum of excitations of the interquark potential [3,4], heavy hybrids [5,6], and the fine structure of the quarkonium spectrum [7]. They are also expected to be a powerful tool in extracting excited-state signals, obtaining high-momentum form factors, pushing thermodynamic calculations to higher temperatures, and in the calculation of transport coefficients.

In this paper, we consider one formulation of the anisotropic action for the pure Yang-Mills sector [8,9]:

$$S_n=-\beta\sum_{x,s>s'}\chi_0^{-1}\left\{\frac{5}{3}\frac{P_{s,s'}}{u_s^4}-\frac{1}{12}\frac{R_{ss,s'}}{u_s^6}-\frac{1}{12}\frac{R_{s's',s}}{u_s^6}\right\}-\beta\sum_{x,s}\chi_0\left\{\frac{4}{3}\frac{P_{s,t}}{u_s^2u_t^2}-\frac{1}{12}\frac{R_{ss,t}}{u_s^4u_t^2}\right\}.$$

Here s,s' run over spatial directions, $P_{s,s'}$ is a 1×1 plaquette, and $R_{s's',s}$ is a 2×1 rectangle. The coefficients of these terms are chosen so that the action has no $O(a_s^2)$ discretization errors in tree-level perturbation theory. χ_0 is the anisotropy parameter and is equal to the aspect ratio of the spatial and temporal lattice spacings, a_s and a_t at the tree level. At higher orders in the perturbative expansion, this aspect ratio receives quantum corrections, so a renormalized anisotropy determined from a physical process, χ_R, differs from χ_0 at $O(\alpha_s)$. Tadpole improvement (TI) of the perturbative expansion is achieved by tuning the input spatial and temporal link parameters u_s and u_t for self-consistency at each choice of β and χ_0.

Here we report on the accurate determination of the tadpole parameters in the plaquette and landau mean-link formulations. (Nontadpole-improved actions have been studied in Refs. [10,11].) We compare methods for measuring the renormalized anisotropy and discuss the importance of lattice artifacts. In order that the anisotropic formulation can be used with confidence, physically distinct methods for determining the renormalized anisotropy $\chi_R=a_s/a_t$ should agree. Discrepancies in the results for χ_R give a measure of lattice artifacts and an indication of the importance of further improvements. Our results have been used in applications of anisotropic lattices to heavy quark hybrid states.

In Sec. II we report on the determination of the tadpole parameters, in Sec. III the renormalized anisotropy measure-

*Present address: Dept. of Physics, UCSD, La Jolla, CA 92093-0319.

TABLE I. Self-consistent plaquette tadpole parameters.

β_P	χ_0	u_s^*	$(u_s^*)^4$	$\langle P_{s,s'}\rangle$ at u_s^*
2.1	6	0.774166	0.3592	0.359136(72)
2.3	4	0.793925	0.3973	0.397267(52)
2.3	6	0.791062	0.3916	0.391621(73)
2.3	10	0.789695	0.3889	0.388650(85)

ments are presented, and in Sec. V we discuss the results and present one conclusions.

II. TADPOLE PARAMETERS

In both the plaquette and Landau mean-link formulations, the tadpole parameters are determined self-consistently and are defined by

$$u_s=(P_{s,s'})^{1/4},\quad u_t=1,\quad \text{plaquette},$$
$$u_s=\langle U_s\rangle_{Landau},\quad u_t=\langle U_t\rangle_{Landau},\quad \text{Landau}, \tag{2.1}$$

where the Landau gauge is defined by the field configuration which maximizes [12]

$$F(\{U\})=\sum_{x\mu}\frac{1}{u_\mu a_\mu^2}\mathrm{Re\,Tr}\left\{U_\mu(x)-\frac{1}{16u_\mu}U_\mu(x)U_\mu(x+\hat{\mu})\right\} \tag{2.2}$$

with respect to gauge transformations. We denote the gauge coupling in the two schemes as β_L and β_P, respectively.

A. Plaquette tadpoles

In the plaquette scheme of Eq. (2.1), $u_t=1$ and u_s is determined self-consistently. The expectation value of the spatial plaquette is computed for a range of input parameters u_s close to and spanning the self-consistent value u_s^*. A linear interpolation is sufficient to give an accurate value of u_s^*. This value is then checked in a further Monte Carlo simulation. The values of u_s^* for a set of couplings β_P and tree-level anisotropies χ_0 are given in Table I. For the lattice sizes used in the simulation, the plaquette expectation value is found to be independent of the volume at the four-significant-figure level. An extrapolation to infinite volume is unnecessary.

B. Landau gauge fixing

The maximization of $F(U_\mu^g)$ in Eq. (2.2), where $U_\mu^g=g(x)U_\mu(x)g^\dagger(x+\mu)$ with respect to a gauge transformation $\{g(x)\}$, was carried out using the conjugate-gradient method modified to deal with the group structure of the link elements. At each stage of the iteration the appropriate conjugate-gradient vector $\{\boldsymbol{v}(x)\}$ is computed as a covariant derivative [13]:

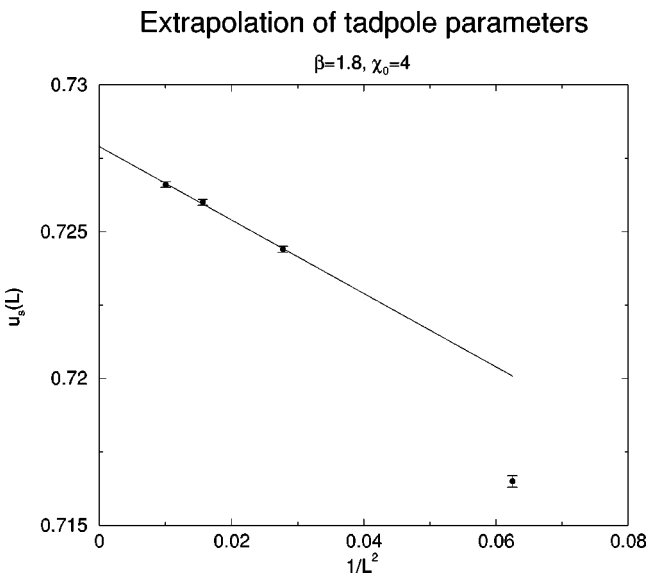

FIG. 1. Fit of $u_s(L)=u_s(\infty)+A_s/L^2$ for $L=6,8,10$.

$$\boldsymbol{v}(x)=\frac{\partial}{\partial\eta(x)}F(U_\mu^g)|_{\eta=0}, \tag{2.2$'$}$$

where $g(x)=e^{\eta(x).T}$ and T are the generators of $SU(3)$. The vector $\{\boldsymbol{v}(x)\}$ has elements lying in the Lie algebra of $SU(3)$. For each vector a series of group elements is constructed in the associated one-parameter subgroup, each element being a given power of the preceding one:

$$g_1=\exp(\epsilon\boldsymbol{v}),\quad g_n=(g_{n-1})^p,\quad 1<n\leqslant N. \tag{2.2$''$}$$

The local maximum in the direction $\boldsymbol{v}$ is found by evaluating $F(U_\mu^{g_p})$ in descending order from $p=N$ to $p=1$. The value of ϵ, at any stage, is reduced until either the sequence exhibits a maximum or remains constant within a preset tolerance.

For large χ_0 the terms including U_t dominate the expression for F and near to the maximum relatively small changes in F correspond to quite large changes in u_s. Consequently, to be sure that u_s as well as u_t is accurately calculated, the maximum must be found to a sufficiently high accuracy. The criterion chosen was $\delta F/F\leqslant 2\times10^{-6}$ where δF was the accumulated change in F for three consecutive iterations of the conjugate-gradient algorithm for which the individual changes in F were nonzero. This criterion accounts for the observation that from time to time close to the maximum the change in F was zero. We chose $\epsilon=2\times10^{-5}$, $p=4$, and $N=6$.

C. Landau gauge fixed tadpoles

The self-consistent value of $\boldsymbol{u}=(u_s,u_t)$ can be determined by a generalized Newton-Rapheson method or by linear interpolation. The latter method was used for the mean-link tadpoles and was implemented by choosing four input tadpoles $\boldsymbol{u}_i$, $i=1,\ldots,4$, and measuring the four corresponding output tadpoles $\boldsymbol{u}_i'$, $i=1,4$. A linear map is assumed for the incremental vectors $\mathbf{r}_i=(\boldsymbol{u}_i-\boldsymbol{u}_1),\rightarrow\mathbf{r}_i'=(\boldsymbol{u}_i'-\boldsymbol{u}_1')$, $i=2,3,4$:

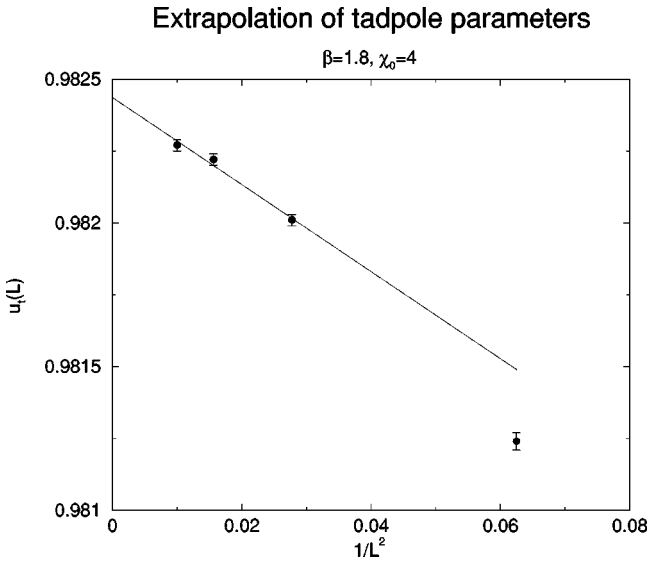

FIG. 2. Fit of $u_t(L)=u_s(\infty)+A_t/L^2$ for $L=6,8,10$.

$$\mathbf{r}_i = \boldsymbol{M}\mathbf{r}_i', \quad i=2,3,4, \tag{2.3a}$$

where $\boldsymbol{M}$ is a 2×2 matrix that is determined from the measured images of $\mathbf{r}_2,\mathbf{r}_3$ and checked for consistency against the measured image of $\mathbf{r}_4$. The self-consistent tadpole $\boldsymbol{u}^*$ is then predicted to be

$$\boldsymbol{u}^* = \boldsymbol{u}_1 + (1-\boldsymbol{M})^{-1}(\mathbf{r}_1' - \mathbf{r}_1). \tag{2.3b}$$

The self-consistency of $\boldsymbol{u}^*$ is then checked computationally. This method was found to be very reliable and only subject to minor adjustments to account for statistical errors.

Moreover, a meaningful statistical error can be assigned to $\boldsymbol{u}^*$ from the image under M^{-1} of the statistical error box deduced for $\boldsymbol{u}^*$ from the measurements values of the tadpole parameters. Let the image of $\boldsymbol{u}^*$ under the map M be $\boldsymbol{u}^{*\prime}$ with statistical error $\delta\boldsymbol{u}^*$. The value $\boldsymbol{u}^*$ is acceptable if in terms of components $\boldsymbol{u}^{*\prime}-\delta\boldsymbol{u}^{*\prime}<\boldsymbol{u}^{*\prime}<\boldsymbol{u}^{*\prime}+\delta\boldsymbol{u}^{*\prime}$, and the error quoted on $\boldsymbol{u}^*$ is $\delta\boldsymbol{u}^*=M^{-1}\delta\boldsymbol{u}^{*\prime}$. A typical example is for $\beta_L=1.8$, $\chi_0=4$ on a $6^3\times 24$ lattice where

$$\boldsymbol{M}^{-1}=\begin{pmatrix} 0.341 & -0.227 \\ -0.033 & 0.957 \end{pmatrix},$$

$$\delta\boldsymbol{u}^{*\prime}=\begin{pmatrix} 3\times 10^{-4} \\ 3\times 10^{-5} \end{pmatrix} \Rightarrow \delta\boldsymbol{u}^*=\begin{pmatrix} 1\times 10^{-4} \\ 2\times 10^{-5} \end{pmatrix}. \tag{2.3c}$$

In practice it is found that the error in u_s^* is typically reduced by a factor of 3 compared with the statistical error from the simulation verifying the self-consistency.

The simulation for the mean-link tadpoles was done on the Hitachi SR2201 computers at the Cambridge High Performance Computing Facility and the Tokyo University Computer Center. The lattices used were $L^3\times T$ with $T=\chi_0 L$ and $L=6,8$ in all cases except one. The high accuracy demanded by the maximization process was very time consuming, requiring many configurations for statistical accuracy. Consequently, only one example with $L=10$ was done as a check on the finite-size scaling ansatz $\boldsymbol{u}^*(L)=\boldsymbol{u}^*(\infty)+A/L^2$. Typically, for $10^3\times 40$ about 400 conjugate-gradient iterations were needed taking about 60 s per iteration. In the cases $L=6,8,10$ for $\beta_L=1.8$, $\chi_0=4$, the fit to the finite-size scaling ansatz was very good as can be seen in Figs. 1 and 2. For other cases the linear extrapolation was assumed to hold. The values measured for $\boldsymbol{u}^*(L)$ and the extrapolation to $L=\infty$ are given in Table II.

III. ANISOTROPY

In this section we report on two methods for determining χ_R. The first uses the dispersion relation for the torelon [14] and the second uses the comparison of the potential measured in the fine and coarse directions using Wilson loops.

A. Torelon

The lattice considered is $S^2\times L\times T$ with typical values $S=8$ in the x and y directions, $L=3,4,5$ in the z direction, and $T=50$ in the fine or t direction. The lattice has periodic boundary conditions and the torelon is created by a Polyakov line that loops around the lattice in the z direction. The Polyakov line is associated with a particular point in the

TABLE II. Self-consistent Landau mean-link tadpole parameters for various lattice sizes L, including the $1/L^2$ extrapolation to $L=\infty$.

		L				
β_L	χ_0	4	6	8	10	∞
1.8	4	0.7165(2) 0.98124(3)	0.7244(1) 0.98201(2)	0.7260(1) 0.98222(2)	0.7266(1) 0.98227(2)	0.7279(2) 0.98243(3)
1.8	6	0.7115(2) 0.99167(3)	0.7191(1) 0.99194(2)	0.7202(1) 0.99200(1)	– –	0.7216(3) 0.99208(3)
1.7	4	– –	0.7127(1) 0.98105(2)	0.7143(1) 0.98188(2)	– –	0.7164(3) 0.98295(5)
1.7	6	– –	0.7075(1) 0.99149(1)	0.7086(1) 0.99153(1)	– –	0.7100(3) 0.99158(3)

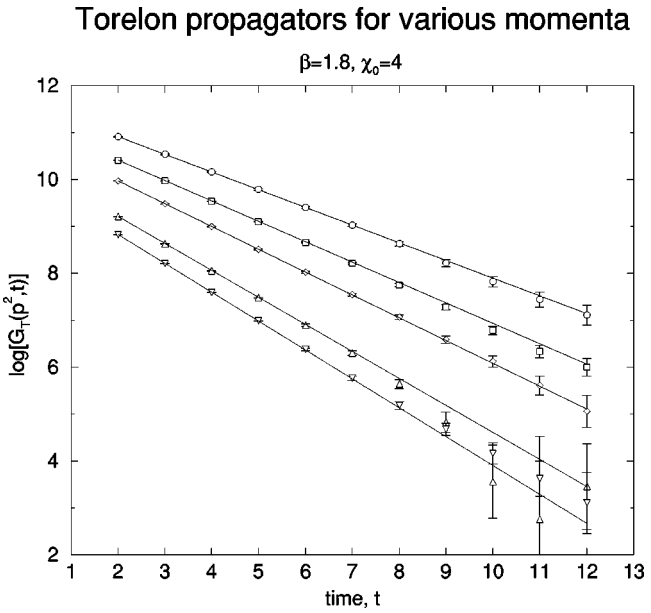

FIG. 3. Fit of the relativistic dispersion, Eq. (3.1d), to the torelon propagators for $\boldsymbol{p}^2=\boldsymbol{n}^2(\pi/4)^2$ for $\boldsymbol{n}^2=0,1,2,4,5$ corresponding, respectively, to the curves from the top downwards. The fit has $\chi^2/N_{\rm df}=0.96$ with $(M_T a_s)^2=1.85(4)$, $\chi_R=3.61(2)$.

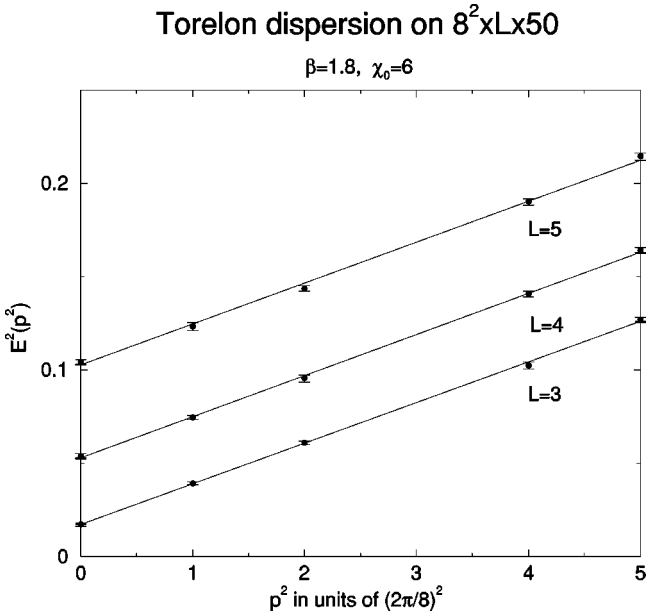

FIG. 4. Plots of $E(\boldsymbol{p}^2)$ versus $\boldsymbol{p}^2$ for $L=3,4,5$ on an $8^2\times L\times 50$ lattice. The lines show the fit to $E(\boldsymbol{p}^2)=A+B\boldsymbol{p}^2$.

(x,y) plane and is constructed from links which are covariantly smeared in a manner similar to APE smearing:

$$T(x,y,t)=\mathrm{Tr}\prod_{z=0}^{z=L-1} W_z(x,y,z,t),$$

$$W_z(x,y,z,t)=\left(1+\frac{l^2D^2}{4m}\right)^m U_z(x,y,z,t), \qquad (3.1a)$$

where D is the appropriate covariant derivative. Typically, $l=1.5$, $m=10$. The state with momentum $\boldsymbol{p}=(p_x,p_y)=(n_x,n_y)(2\pi/Sa_s)$ is

$$T(\boldsymbol{p},t)=\sum_{x,y} T(x,y,t)e^{i(p_x x+p_y y)}. \qquad (3.1b)$$

The torelon propagator

$$G_T(\boldsymbol{p},t)=\frac{1}{T}\sum_{t'=0}^{t'=T-1}\langle T(\boldsymbol{p},t')T^*(\boldsymbol{p},t+t')\rangle \qquad (3.1c)$$

is measured for various choices of momentum $\boldsymbol{p}$ and a correlated simultaneous fit using SVD decomposition is made to the relativistic dispersion formula:

$$G_T(\boldsymbol{p},t)=c(\boldsymbol{p})e^{-E(\boldsymbol{p})a_t\bar{t}},$$

$$E(\boldsymbol{p})a_t=\frac{a_s\sqrt{\boldsymbol{p}^2+M_T^2}}{\chi_R}, \qquad (3.1d)$$

where M_T is the torelon mass and $\bar{t}=t/a_t$. The momenta used were $\boldsymbol{n}^2=n_x^2+n_y^2=0,1,2,4,5$ with $S=8$. An example of the fit obtained is shown in Fig. 3 for $\beta_L=1.8$, $\chi_0=6$. The fit is over the range $2\leqslant t\leqslant 12$ and has $\chi^2/N_{\rm df}=0.96$ for 43 degrees of freedom (DOF). The fit is good and gives $(M_T a_s)^2=1.85(4)$, $\chi_R=3.61(2)$. In Fig. 4 the dispersion curves $E(\boldsymbol{p}^2)$ versus $\boldsymbol{n}^2$ are plotted for $\beta_L=1.8$, $\chi_0=4$, $L=3,4,5$. From both Figs. 3 and 4 it is clear that rotational invariance is established in the coarse xy directions. The good simultaneous fit to the torelon propagators in all cases shows that the continuum dispersion is well satisfied for momenta at any angle to the coordinate axes.

In Table III we give the full set of results for the torelon anisotropies we have measured. There is no noticeable dependence within errors of χ_R on L and the dependence on β is small for the two values of β used.

From the values $M_T(La_s)$ we can determine the string tension, σ in units of a_s^{-2}. We assume that $M_T(La_s)=\sigma(La_s)La_s$ where $\sigma(La_s)$ is the string tension modified by finite-size corrections [15,16]: $\sigma(La_s)=\sigma+D/(La_s)^2$. A plot of $\sigma(La_s)a_s^2$ versus $1/L^2$ is shown in Fig. 5 with a linear fit which has $\chi^2/N_{\rm df}=0.05$ with $\sigma a_s^2=0.394(3)$. In another calculation we have determined the absolute value of a_t in MeV by computing the splitting $\Delta M_{PS}=M_\Upsilon(1P)-M_\Upsilon(1S)$ for the Υ meson system using $O(mv^6)$ nonrelativistic QCD (NRQCD) [17]. In Table IV we give a_t^{-1}, a_s^{-1}, σa_s^2, the coefficient D, and $\sqrt{\sigma}/\Delta M_{PS}$. This latter ratio is experimentally close to unity but in Ref. [17] using isotropic $\beta=6.2$ UKQCD configurations this ratio was found to be about 1.25 which, from Table IV, agrees with our finding except possibly for the $(\beta=1.7,\chi_0)$ lattice which has the most coarse lattice spacings. It is generally accepted that the discrepancy is due to quenching and the significant outcome is that our results from the anisotropic lattice agree well with those of a spatially finer isotropic lattice of $a=0.06$ fm, indicating that we have correctly reproduced the physics expected for this comparison on lattices with $a_s=0.25$–0.30 fm. A naive estimate for the coefficient D is

TABLE III. Renormalized anisotropies and dimensionless torelon masses for various values of β_L and χ_0 from a simultaneous fit on $8^2\times L\times 50$ lattice.

β_L	χ_0	L					
		3		4		5	
		χ_R	$(M_T a_s)^2$	χ_R	$(M_T a_s)^2$	χ_R	$(M_T a_s)^2$
1.8	4	3.61(1)	0.683(1)	3.61(3)	1.85(4)	3.57(5)	3.39(13)
1.8	6	5.32(2)	0.502(1)	5.28(3)	1.49(3)	5.28(5)	2.84(9)
1.7	4	3.56(2)	1.16(2)	3.56(4)	2.86(9)	3.66(9)	5.51(36)
1.7	6	5.28(2)	0.89(2)	5.28(5)	2.36(6)	5.26(6)	4.25(13)

obtained by calculating the contribution to $M(L)$ from the zero-point fluctuations of the torelon regarded as a periodic flux tube. The outcome is $D=-\pi/3\sim-1.05$ which is compatible with our fit of $D\sim-1.35(5)$. The same calculation predicts that there is no L-independent constant contribution to $M(L)$ and this is verified by our fits.

The torelon dispersion relation was also studied on the plaquette-tuned parameters. For these simulations, lattices of extent $(8\times 10)\times 4\times N_t$ were used to enable us to investigate a wider range of momenta combinations. At momenta close to the cutoff, we expect the discretization errors to be $O(a_s^4p^4,\alpha_s a_s^2p^2)$; thus, in order not to contaminate our determination of χ_R with large discretization errors, we first determined the range of momenta over which a good correlated fit to the continuum dispersion relation could be made. The data for different momentum ranges from simulations at $\beta_P=2.1$, $\chi_0=6$ were tested and these results are shown in Table V. Both the measured anisotropy renormalizations and the torelon rest energies determined are all consistent within

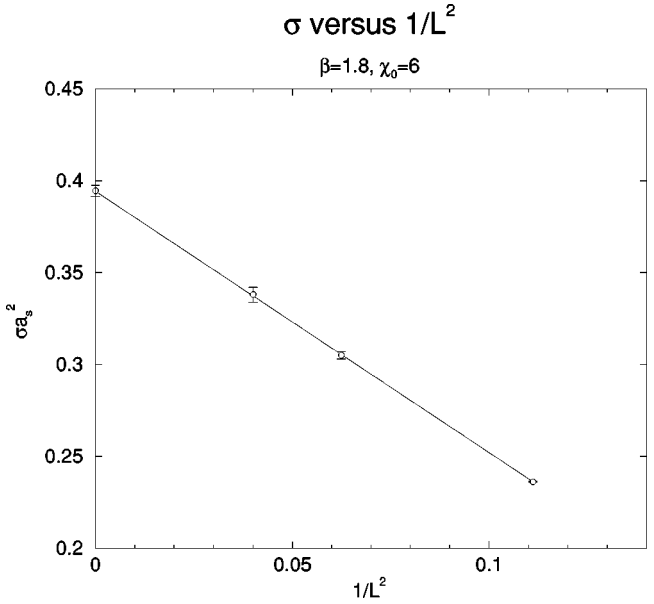

FIG. 5. $\sigma(L)$ versus $1/L^2$ for $\beta_L=1.8$, $\chi_0=6$, with a linear fit giving $\sigma a_s^2=0.394(3)$.

TABLE IV. The inverse lattice spacings for mean-link tadpole-improved actions from the $O(mv^6)$ NRQCD measurement of $\Delta M_{PS}=M_\Upsilon(1P)-M_\Upsilon(1S)$ to determine a_t^{-1} and using the torelon anisotropy to infer a_s^{-1}. The string tension is found from the L dependence of the torelon mass using finite-size scaling ansatz $\sigma(La_s)=\sigma+D/(La_s)^2$.

β_L	χ_0	M_b	a_t^{-1} (MeV)	a_s^{-1} (MeV)	σa_s^2	$\sqrt{\sigma}/\Delta M_{PS}$	D
1.8	4	5.32	2876(75)	797(21)	0.422(7)	$\sim$1.18(3)	$-$1.31(6)
1.8	6	4.75	4503(45)	839(9)	0.394(3)	1.19(2)	$-$1.42(3)
1.7	4	5.97	2353(38)	661(11)	0.513(12)	1.08(2)	$-$1.39(13)
1.7	6	5.56	4112(150)	779(28)	0.469(8)	1.21(5)	$-$1.38(8)

statistical precision up to the highest momentum measured. For the subsequent computations of the anisotropy, presented in Table VI, the largest momentum used was the (1,1) data (shown in boldface in Table V).

B. Sideways potential

In the sideways potential method [18,19], a coarse direction z on the anisotropic lattice is chosen to be the time direction. There are then two types of spacelike direction, coarse and fine. The measurement of the potential between static quarks with a separation lying in the plane of coarse links is compared with the measurement of the potential when the separation lies along the line of fine links. The demand that the two measurements yield the same function of *physical* distance determines the renormalized anisotropy. Points in the coarse-coarse plane are denoted by $\vec{x}=(x,y)$ and points in the fine direction by t where x,y,z,t are integers.

We measure appropriate spatial Wilson loops $W_{ss}(\vec{x},z)$ and also loops using the fine direction $W_{ts}(t,z)$. We define

$$V_s(\vec{x},z)=\log\left(\frac{W_{ss}(\vec{x},z)}{W_{ss}(\vec{x},z+1)}\right),$$

$$V_t(t,z)=\log\left(\frac{W_{ts}(t,z)}{W_{ts}(t,z+1)}\right). \tag{3.2a}$$

TABLE V. Dependence of the renormalized anisotropies and torelon masses on the highest momentum used in the fit to Eq. (3.1d) at $\beta_P=2.1$, $\chi_0=6$.

Maximum (p_x,p_y)	χ_R/χ_0	a_tM_T	$\chi^2/N_{\rm df}$
(1,1)	**0.949(25)**	0.2884(17)	1.19
(0,2)	0.972(23)	0.2886(16)	0.99
(1,2)	0.968(17)	0.2885(15)	0.85
(2,1)	0.976(14)	0.2885(15)	0.89
(2,2)	0.970(11)	0.2883(14)	0.96

TABLE VI. Renormalized anisotropies for various values of β_P and χ_0 using plaquette-tuned mean-link parameters.

β_P	χ_0	χ_R/χ_0	$\chi^2/N_{\rm df}$
2.3	4	0.941(13)	1.04
2.3	6	0.954(23)	0.74
2.3	10	0.940(13)	1.41
2.1	6	0.949(25)	1.19

As $z\to\infty$, $V_s(\vec{x},z)\to V_s(|\vec{x}|)$ and $V_t(t,z)\to V_t(t)$ where $V_s(|\vec{x}|)$ and $V_t(t)$ are the two versions of the interquark potential. For a physical distance r we have $|\vec{x}|a_s=ta_t=r$. We therefore estimate the renormalized anisotropy χ_R by tuning it so that $V_s(|\vec{x}|)=V_t(t/\chi_R)$, where the right side is evaluated by means of linear interpolation between the values measured at integral t. It is implicit in the method that there is effective rotational invariance in the $\vec{x}$ plane. We find that if we exclude potentials at the smallest distances, $|\vec{x}|=1,\sqrt{2}$, then the values of χ_R associated with different directions in the $\vec{x}$ plane generally agree within errors. The agreement is particularly good if the links are smeared in an appropriate manner. The results for the renormalized anisotropy χ_R for both mean-link and plaquette schemes are shown in Table VII.

An alternative approach to making the comparison is to fit the measured potentials with the forms

$$a_sV_s(\vec{x})=a_sV_0+\sigma a_s^2x+\frac{e}{x},$$

$$a_sV_t(t)=a_sV_0+\sigma a_sa_tt+\frac{a_se}{a_tt}. \qquad (3.2b)$$

The renormalized anisotropy χ_R is then determined from the ratio of the coefficients of the linear terms in the two cases. χ_R can in principle be determined from the ratio of the coefficients of the Coulombic terms; however, such an estimate depends on short distance effects and is inherently more sensitive to discretization errors.

This approach was tested on an $8^3\times48$ lattice at $\beta_P=2.3,\chi_0=6$. Prior to measurement, the lattice is blocked to an 8^4 volume by thinning the time slices of spatial links and replacing the temporal links with the product of six fine links connecting the appropriate time-slices. The t and z axes are then interchanged, since as before we want to use a coarse direction for Euclidean decay. Then a standard APE-smearing algorithm is applied to links on the new time slices. These degrees of freedom are then used to measure the potential in the (x,y) and z axes in the standard fashion. Figure 6 shows the results of this simulation. The best fits of this data to Eq. (3.2b) for a range of static-source separations were computed and the string tension results are shown in Table VIII. In fit C, the Coulomb term was poorly resolved and was thus fixed to zero. The use of these different ranges allowed us to investigate the systematic uncertainty and discretization errors in determining χ_R from this method. The three results are consistent within 2%. The anisotropy measurement from the full range of separations (fit A, shown in boldface in Table VIII) is in good agreement with the torelon dispersion result of Table VI.

TABLE VII. Results for the renormalized anisotropy, χ_R, using the sideways potential method for both mean-link and plaquette tadpole-improved schemes

Mean link			Plaquette		
β	χ_0	χ_R	β	χ_0	χ_R
1.8	4	3.67(2)	2.1	6	5.80(5)
1.8	6	5.48(3)	2.3	4	3.95(3)
1.7	4	3.67(3)	2.3	6	5.93(5)
1.7	6	5.40(5)	2.3	10	10.00(20)

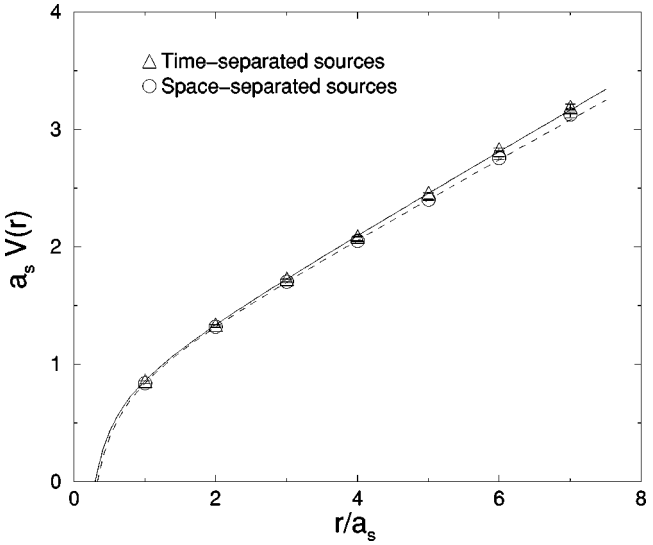

FIG. 6. The potential at $\beta_P=2.3$, $\chi_0=6$ between static sources separated along both spatial and temporal axes.

Both the above approaches yielded results reasonably consistent with each other and with the toleron results at the 3% level. Discrepancies can easily be explained by the presence of discretization errors. Because the flux tube generating $V_s(|\vec{x}|)$ has a coarse-fine cross section and that generating $V_t(t)$ a coarse-coarse cross section we anticipate, as in the case of the toleron [Eq. (4.5)], that some discretization error in χ_R that is $O(\alpha_s(a_s/R)^2)$ will remain. Since $a_s\sim0.3$ fm, $R\sim0.71$–1 fm, and $\alpha_s\sim0.3$, we expect discretization errors to be around 5%.

Because we are concerned to make the long distance behavior consistent in both the fine and coarse directions, it is advantageous to use Wilson loops of the largest possible spatial extent. However, in practice, the statistical errors in large Wilson loops grow exponentially with separation. In order to achieve acceptable errors we were restricted to using loops of size 2 or 3 in coarse lattice units. This is to be compared with the torelon, where the practical size is 3 or 4 lattice units.

TABLE VIII. Results for the renormalized anisotropy, χ_R from fits to the static potential. In fit C, the Coulomb term was set to 0.

Fit	Separations	σa_s^2	$\chi^2/N_{\rm df}$	$6\sigma a_s a_t$	$\chi^2/N_{\rm df}$	χ_R/χ_0
A	1-7	0.3293(33)	1.13	0.3492(26)	1.21	**0.943(12)**
B	1-4	0.3315(60)	0.85	0.3526(64)	1.14	0.940(24)
C	3-7	0.3506(32)	0.70	0.3664(34)	1.11	0.957(12)

IV. DISCRETIZATION ERRORS

One way of viewing discretization errors is to regard them as arising from the absence of the correction term in the lattice action that yields continuum results. The corresponding term in the action density can be presumed to be a local operator. The locality of the operator implies that while there may be a correction to the mass per unit length of the torelon, there is no correction that directly alters the asymptotic proportionality of the torelon mass and its length. The appropriate length scale against which to measure lattice artifacts therefore is the radius R of the toleron cross section or, equivalently, Λ_{QCD}^{-1} or $\sqrt{\sigma}$ where σ is the string tension. We expect therefore that the $O(a_s^2)$ errors in χ_R are proportional to $(a_s/R)^2$.

A persuasive plausibility argument for this behavior is as follows. The torelon state of momentum $\boldsymbol{p}$ and mass M_T is an eigenstate of the transfer matrix T with an eigenfunctional labeled by $\boldsymbol{p}$ and M_T and eigenvalue $\exp[-E(\boldsymbol{p}^2)a_t/\chi_R]$. Suppose an operator is added to the action which corrects for the $O(\alpha_s a_s^2)$ errors. This operator will be local on the scale of the lattice and the effect on $E(\boldsymbol{p}^2)$ can be estimated using first-order perturbation theory:

$$\delta\frac{a_s E(\boldsymbol{p}^2)}{\chi_R}=\alpha_s f(\overline{\boldsymbol{p}^2},\overline{M}_T), \tag{4.1}$$

where $\overline{\boldsymbol{p}^2}=\boldsymbol{p}^2 a_s^2$, $\overline{M}_T=M_T a_s$, and $f(\overline{\boldsymbol{p}^2},\overline{M}_T)$ is the dimensionless matrix element of the added operator which is proportional to a_s^2 by construction. The question is what scale balances the dimension of a_s^2. We find

$$-\frac{\delta\chi_R}{\chi_R^2}=\alpha_s\phi'(0,\overline{M}_T), \tag{4.2}$$

$$\frac{\delta\overline{M}_T^2}{\chi_R}=\alpha_s[\,\phi(0,\overline{M}_T)-\overline{M}_T^2\phi'(0,\overline{M}_T)], \tag{4.3}$$

where $\phi(\overline{\boldsymbol{p}^2},\overline{M})=a_s E(\boldsymbol{p}^2) f(\overline{\boldsymbol{p}^2},\overline{M}_T)$ and $\phi'=\partial\phi/\partial(\overline{\boldsymbol{p}^2})$. It must be that the change in the action by a local operator corresponds to a change in the string tension, σ. Hence, since $M_T=\sigma L$, it follows that $\delta\overline{M}_T^2\propto\overline{M}_T^2$ as this is the only parameter depending on L, and from Eq. (4.3) this implies that

$$\phi(0,\overline{M}_T)\sim\overline{M}_T^2,\quad \phi'(0,\overline{M}_T)\sim\overline{M}_T\text{-independent constant}. \tag{4.4}$$

It is conceivable that an accidental cancellation between the two terms in Eq. (4.3) would allow different behavior to be inferred for ϕ and ϕ' but these results must hold true for all possible local perturbations, not just the particular one that eliminates $O(\alpha_s a_s^2)$ errors. We consider this kind of cancellation to be unlikely. Substituting this behavior for ϕ' into Eq. (4.2) we find that

$$\frac{\delta\chi_R}{\chi_R^2}\sim C\frac{a_s^2}{R^2}, \tag{4.5}$$

where R is a typical length scale associated with the torelon which cannot be M_T^{-1}, for example, the flux tube radius. Alternatively, R^{-1} can be taken to be $\sqrt{\sigma}$, Λ_{QCD}.

V. CONCLUSIONS

In this paper we have investigated various methods for measuring the renormalized aspect ratio for pure QCD on an anisotropic lattice. In the main we used a tadpole-improved action with the Landau gauge mean-field definition for the tadpole parameters, but we also included results for the action with tadpoles defined by the mean plaquette. The object of the investigation was to assess the consistency of different methods in order to judge the effectiveness of the improvement scheme. In principle, measurements of the anisotropy from different physical probes should agree close to the Euclidean-symmetric continuum limit. The bare anisotropy χ_0 is renormalized by the effect of operators which are irrelevant in the neighborhood of the fixed point controlling the continuum limit. From a renormalization group (RG) view point the location of this fixed point is ambiguous up to redefinitions of the RG transformation used to locate it. This ambiguity is due to redundant operators [20–22] which have no effect on physical observables of the continuum theory. Consequently, continuum actions with different χ_R can differ only by redundant operators since they must correspond to the same continuum physics. Thus, while χ_R can be changed by tuning χ_0, an action with no lattice artifacts must give rotationally invariant physical results and, consequently, any physical method for measuring χ_R, such as the ratio of two physical observables, must give the same answer. Inasmuch as this is not the case the differences will give an estimate for the effect of lattice artifacts and the necessity for improvement.

The spatial lattice spacing a_s was measured in a separate NRQCD simulation by fitting the $1P$-$1S$ mass-splitting ΔM_{PS} for bottomonium. This estimate can be compared with the string tension, deduced from a D/L^2 extrapolation to ∞ of the torelon mass. The coefficient D was found to be ~ -1.38 which is in tolerable agreement with $-\pi/3$ pre-

dicted from analysis of flux-tube fluctuations [16]. The ratio $\sqrt{\sigma}/\Delta M_{PS}$ is ~ 1.2, in agreement with earlier NRQCD analyses [23,17]. The departure from the experimentally observed value of ~ 1 is attributed to quenching. The values for both the mean-link and plaquette tadpoles were found self-consistently. This was very resource intensive in the mean-field case since it required a very accurate gauge fixing to the Landau gauge and the self-consistent iteration is in the 2D space of (u_s, u_t) which requires additional effort. Also, for given χ_0 the tadpoles showed an L dependence and hence required an extrapolation to $L=\infty$. This in turn requires accurate data for a good fit. In contrast, the plaquette tadpole was easily found and there was no discernible L dependence.

The torelon method deduces χ_R from a fully correlated fit to the dispersion relation. Statistical errors are produced by the fit. The sideways potential approach requires some method for matching the coarse and fine potentials and the error analysis is more complex because of both systematic and statistical errors and because the signal rapidly decreases as the loop size increases. Two methods were used to extract χ_R. The first compared the loop predictions for the coarse and fine potentials (3.2a) and deduced χ_R from the rescaling of t needed for them to agree. This method was applied to actions with mean-field improvement. Typical loops were of edge length 2–3 in units of the coarse spacing a_s. There is a clear difference in results compared with the torelon computation of about 3–4 %. In the second approach the fine direction is first blocked by a scaling of χ_0 to give a lattice that is approximately isotropic and then the potential is fitted to a standard form (3.2b) and χ_R deduced by requiring that the linear slopes agree. The latter method has the advantage that it depends only on the long-range structure of the potential and excludes the short range Coulomb part. However, it does require large computing resources to extract a reliable signal at large separations, in this case up to 7 lattice units. This technique was applied mainly to actions with plaquette improvement. Although less extensively investigated, the results are consistent with the torelon computation.

From Table III we see that χ_R deduced from the torelon measurement is independent of L. This is to be expected since measurements of χ_R should not be sensitive to the finite volume when deduced from physical observables. We therefore expect the same to be true when χ_R is derived from the sideways potential. It is known, in any case [6], that finite-volume effects are negligible for measurements of potentials for even relatively small lattices. We are consequently confident that the finite-volume effects are negligible in our work except where we have explicitly exhibited them, namely, in the extrapolation of the mean-link tadpole values to $L=\infty$ and in the discussion of the string tension.

The observed discrepancies can be easily attributed to residual lattice artifact effects. For the torelon we expect $\delta\chi_R/\chi_R \sim C\alpha_s a_s^2/R^2$ which can be sizable although C is unknown. However, it should also be remarked that neither the torelon nor the second sideways potential method include the Coulomb part of the static potential. Because of its short-range nature, this part will be the most sensitive to the effect of lattice artifacts. In this case agreement of the predictions for χ_R is good. This may merely indicate that χ_R is being deduced from the properties of the flux tube in both cases and so they should agree in that artifact effects are the same. However, it is encouraging that different methods based on the long-range properties of the action are consistent and it is worth noting that the torelon flux tube was 3–5 lattice units in length whereas it was necessary to extend the potential method to 7 lattice units. Simulation times are correspondingly reduced for the torelon. Unfortunately, it was not possible to apply the second method to data gathered using the mean-field action because of limitations in resources.

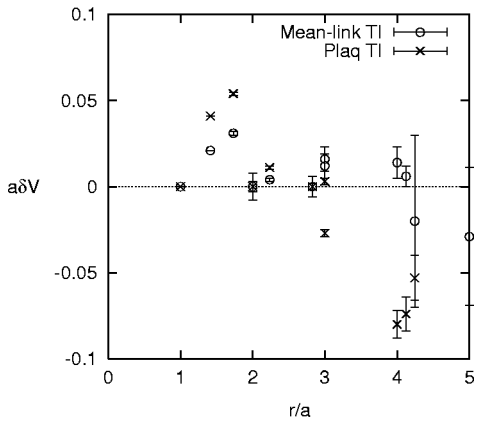

FIG. 7. Deviation of the static potential from the fit, $a \approx 0.29$ fm. Both sets of data are fitted to $V(r)=b+c/r+\sigma r$, using the points $r=1,2,\sqrt{8}$, which therefore show no deviation. For the remaining points, it is clear that mean-link TI (circles) shows smaller rotational symmetry violations than plaquette TI. See also Table IX.

We do not find any evidence that the mean-link-tuned action is superior to the plaquette-tuned action in suppressing lattice artifacts, and it should be noted that the computation required to determine the mean-link tadpoles for the former case is very time consuming. However, there is other evidence that the mean-link action is superior. It is known to give smaller scaling errors in the NRQCD charmonium hyperfine splitting [24,25], better hadron mass scaling [8], and a clover coefficient for SW fermions (with the Wilson gauge action) that agrees more closely [12] with the nonperturbatively determined value [26,27]. Using our configurations we present evidence that it also gives better rotational invariance for the static quark potential. In Fig. 7 we show the deviation

TABLE IX. Comparisons of the normalized deviation from rotational invariance between the Wilson action and the plaquette and mean-link tadpole-improved (TI) actions. The ratios shown are zero in the case where rotational invariance holds, and on these measures the mean-link TI action is superior.

Action	$\frac{V(111)-V_{\text{fit}}(\sqrt{3})}{V(2)-V(1)}$	$\frac{V(221)-V(3)}{V(3)-V(1)}$
Wilson	0.267(2)	0.099(3)
plaquette TI	0.091(10)	0.027(2)
mean-link TI	0.050(5)	0.003(7)

of the potential from a fit to the standard form $V(r)=b+c/r+\sigma r$. Comparing the mean-link TI data with the plaquette TI data, it is clear that mean-link TI gives smaller deviations from the rotationally invariant fit. In Table IX we present some of the features of Fig. 7 in a quantitative form. As expected, mean-link TI gives better rotational invariance at $r=\sqrt{3}$, and it causes the two $r=3$ potentials [(2,2,1) vs (3,0,0)] to agree better.

As mentioned in the Introduction, there are many applications for anisotropic lattices. It would be valuable to measure anisotropies for a wider variety of lattice spacings and bare anisotropies, using the methods we have investigated. It would also be very useful to calculate perturbative formulas for the anisotropy and lattice spacing as a function of the bare parameters of the action, β and χ_0 [10,11,28]. Finally, it will be necessary to repeat this tuning process for improved light quark actions. Some of the requisite perturbative calculations have already been performed [29].

ACKNOWLEDGMENTS

This work is supported in part by funds provided by the U.S. Department of Energy (DOE) under cooperative research agreement DF-FC02-94ER40818. Part of the calculation was performed on the SP-2 at the Cornell Theory Center, which receives funding from Cornell University, New York State, federal agencies, and corporate partners. Calculations were carried out on the Hitachi SR2201 computers at the University of Cambridge High Performance Computing Facility and the Tokyo University Computer Centre.

[1] C. Morningstar and M. Peardon, Phys. Rev. D **56**, 4043 (1997).
[2] C. Morningstar and M. Peardon, Phys. Rev. D **60**, 034509 (1999).
[3] K. Juge *et al.*, Nucl. Phys. B (Proc. Suppl.) **63**, 326 (1998).
[4] K. Juge *et al.*, Phys. Rev. Lett. **82**, 4400 (1999).
[5] T. Manke *et al.*, Phys. Rev. Lett. **82**, 4396 (1999).
[6] I.T. Drummond *et al.*, Phys. Lett. B **478**, 151 (2000).
[7] T. Manke *et al.*, Nucl. Phys. B (Proc. Suppl.) **86**, 397 (2000).
[8] M. Alford, T.R. Klassen, and G.P. Lepage, Phys. Rev. D **58**, 034503 (1998).
[9] C. Morningstar, Nucl. Phys. B (Proc. Suppl.) **53**, 914 (1997).
[10] G. Burgers *et al.* Nucl. Phys. **B304**, 587 (1988).
[11] S. Sakai *et al.*, hep-lat/0002029.
[12] G.P. Lepage, Nucl. Phys. B (Proc. Suppl.) **60A**, 267 (1998).
[13] I.T. Drummond, S. Duane, and R.R. Horgan, Nucl. Phys. **B220**[FS8], 119 (1983).
[14] M. Teper, Phys. Rev. D **59**, 014512 (1999).
[15] M. Lüscher, Nucl. Phys. **B180**, 317 (1981).
[16] N. Isgur and J. Paton, Phys. Rev. D **31**, 2910 (1985).
[17] S.M. Catterall *et al.*, Phys. Lett. B **321**, 246 (1994).
[18] T.R. Klassen, Nucl. Phys. **B533**, 557 (1998).
[19] J. Engels *et al.*, Nucl. Phys. **B564**, 303 (2000).
[20] F.J. Wegner, J. Phys. C **7**, 2098 (1974).
[21] M.E. Fisher and M. Randeria, Phys. Rev. Lett. **56**, 2332 (1986).
[22] M. Lüscher and P. Weisz, Commun. Math. Phys. **97**, 59 (1985).
[23] S.M. Catterall *et al.*, Phys. Lett. B **300**, 393 (1993).
[24] N.H. Shakespeare and H.D. Trottier, Phys. Rev. D **59**, 014502 (1999).
[25] N.H. Shakespeare and H.D. Trottier. in *Lattice '98* [Nucl. Phys. B (Proc. Suppl.) **73**, 342 (1999)].
[26] R. Sommer, Nucl. Phys. B (Proc. Suppl.) **60A**, 279 (1998).
[27] M. Lüscher *et al.*, Nucl. Phys. B (Proc. Suppl.) **B491**, 323 (1997).
[28] I.T. Drummond *et al.*, ''Analytic two-loop calculation and simulation of anisotropic lattice parameters'' (work in progress).
[29] S. Groote and J. Shigemitsu, Phys. Rev. D **62**, 014508 (2000).